Supplemental Information for: Formation of Lead Halide Perovskite Based Plasmonic Nanolaser and Nanolaser Array by Tailoring the Substrate

Can Huang[1], Wenzhao Sun[1], Yubin Fan[1], Yujie Wang[1], Yisheng Gao[1], Nan Zhang[1], Kaiyang Wang[1], Shuai Liu[1], Shuai Wang[1], Qinghai Song[1, 2, *], Shumin Xiao[1, 2, †]

1. State Key Laboratory on Tunable laser Technology, Ministry of Industry and Information Technology Key Lab of Micro-Nano Optoelectronic Information System, Shenzhen Graduate School, Harbin Institute of Technology, Shenzhen, China, 518055.
2. Collaborative Innovation Center of Extreme Optics, Shanxi University, Taiyuan 030006 China.

* qinghai.song@hit.edu.cn

† shumin.xiao@hit.edu.cn

In the main text, we have experimentally realized the $MAPbX_3$ based spasers and explored the possibility of controlling their emission wavelengths and achieving the spaser array. In this supplemental information, we show all of the experimental details to support the information in the manuscript. This supplemental information includes the following sections.

Section-1: Experimental details for synthesis and optical characterization

1.1.Fabrication of hybrid structure

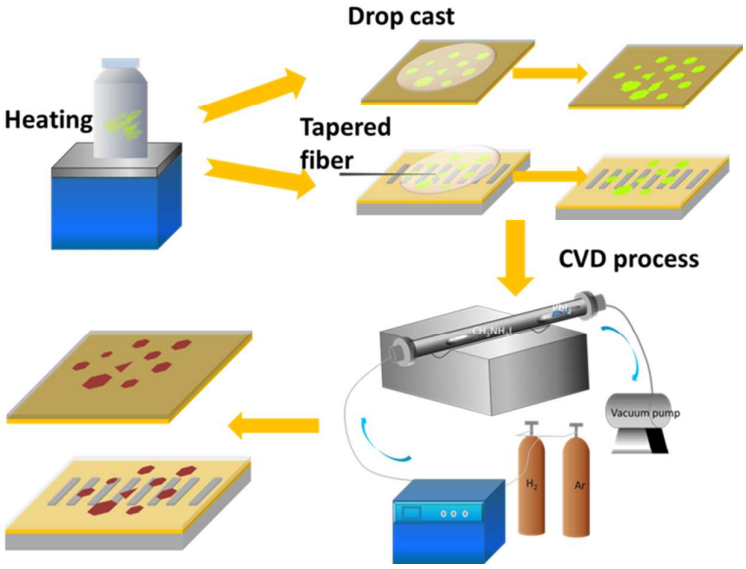

Figure S 1. Schematic of device fabrication process

The basically fabrication process of hybrid structure have been described in the main text. And have been schematically shown in figure S1. Basically, the saturated PbI_2 aqueous solution was prepared by dissolving 2 mg PbI_2 powder in 5 mL of deionization (DI) water and heated at 110 °C for 1 hour and cooled naturally. Then the solution was casted on the SiO_2/Au substrate and the PbI_2 microplate started to appear. Notably, During the evaporation of DI water, the microplates were moved by a tapered fiber equipped with a 3D translation platform to the designed position before the PbI_2 nanocrystals cling to the substrate and dry naturally, while it could also suck the water out slowly with a paper towel. During the whole vapor conversion process, the CH_3NH_3I powder was placed at the center of a low pressure chemical vapor deposition (LPCVD) furnace, while the as-grown PbI_2 microplates on the Au/SiO_2 or silica substrate were mounted downstream of the apparatus. Central heating zone was increased to 125 °C (8 °C/min heating rate, then 10 mins as a buffer) under low-pressure conditions (40−50 Torr) and maintained from 25 min to 2 h. Ar and H_2 were used as carrier gases with flow rates of 35 and 15 sccm, respectively. The furnace was then naturally cooled down to room temperature. Both the perovskite setting on Au/SiO_2 film and perovskite on grating used the same fabrication process.

1.2. Fabrication of the Au/SiO_2 array and Au/SiO_2 disk

The fabrication process of the Au/SiO_2 array have been shown below, A thin negative photoresist (AZ, microchem) film was spin-coated (4000 rpm, 2 mins) onto the silicon substrate and then patterned by standard photolithography. The Au and SiO_2 films were deposited with electron-beam evaporation (0.3 Å/s, 70 nm for Au; 0.3 Å/s, 10nm for SiO_2). After 12 hours immersed in the peel liquid, the AZ microstrips were removed. The pre-synthesized PbI_2 solution was then casted on the SiO_2/Au grating substrate. After the reaction with $CH_3NH_3PbI_3$ using the LPCVD method, we then got the perovskite microplates on Au/SiO_2 grating. While for the Au/SiO_2 disk, the fabrication process is almost the same with the Au/SiO_2 grating, instead of photolithography, the disk was patterned by the EBL (Raith E-line, 30 kV). Basically, the ZEP520A film was first spin-coated (4000 rpm, 2 mins) onto the clean silicon nitride substrate and baked at 180 °C for an hour. then the sample was patterned by EBL and developed in N50 solution for 60 s at 0 °C to form the ZEP nanostructures. After 12 hours immersed in the peel liquid, the ZEP520A film were removed. Figure S 2(b) shows the SEM image of the original Au/SiO_2 disk and figure S 2(c) shows the tilt-view SEM image of Au/SiO_2 disk covered with a perovskite nanosheet.

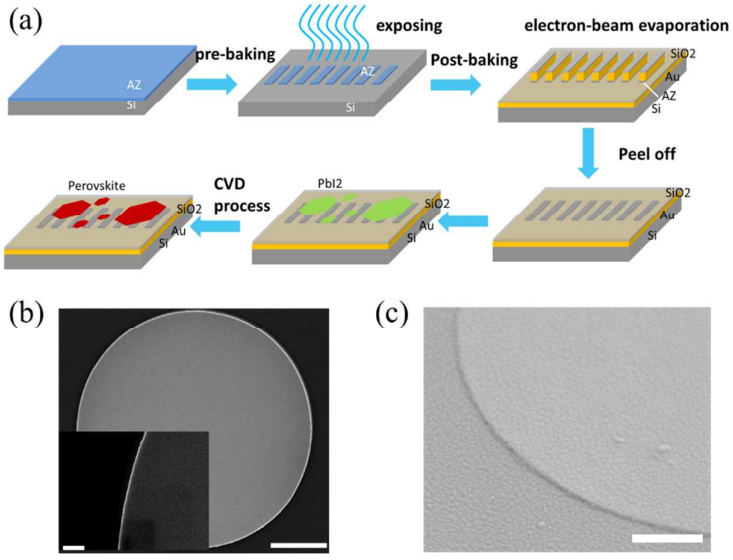

Figure S 2 (a). Fabrication process of spaser array. (b) Original SEM image of the Au/SiO_2 disk, Scale bar: 5 μm. Inset shows the magnified image of the disk edge. Scale bar: 500 nm. (c) The tilt-view SEM image of Au/SiO_2 disk covered with perovskite nanosheet. Scale bar: 3 μm.

1.3. PbI_2 and $MAPbI_3$

For the thicker samples synthesized by vapor-deposition method, the PbI_2 nanosheets usually can't completely be translated to the perovskite nanosheets, the XRD spectrum in the main text have shown that there are part of PbI_2 nanocrystal in the synthesized perovskite nanosheets. We further confirm this by executing TEM experiments on these samples. Figure S3(a) shows the TEM image of the degradation sample under the electron beam. It can be clearly seen the hexagonal nanocrystal presented after irradiation. Figure S3(b) shows the XRD spectrum synthesized simultaneous with the sample in figure S3(a). Four main peaks local at 12.94°, 25.76°, 38.9° and 52.62°, corresponding to (001), (002), (003), (004) of PbI_2 nanocrystal facet,[1] respectively. Other two peaks local at 14.1° and 28.5° corresponding to (110), (220) facet of $CH_3NH_3PbI_3$ nanocrystal, respectively. According to Cao's results,[2] the XRD shown in figure S3(b) confirming the $CH_3NH_3I_3$ nanosheets fractional have been more than 90%. Figure S3(c) shown the high-resolution transmission electron microscopy (HRTEM) of the hexagonal nanocrystal and corresponding selected area electric diffraction (SAED) pattern. The distances between two parallel lines are 0.227 nm and 0.396 nm, confirming the crystal structure well.[3] Figure S3(d) exhibited the XRD pattern of the PbI_2 nanosheets before LPCVD process. Here two peaks local at 14.1^o and 28.5^o disappeared, which correspond to the $CH_3NH_3PbI_3$ microcrystal.

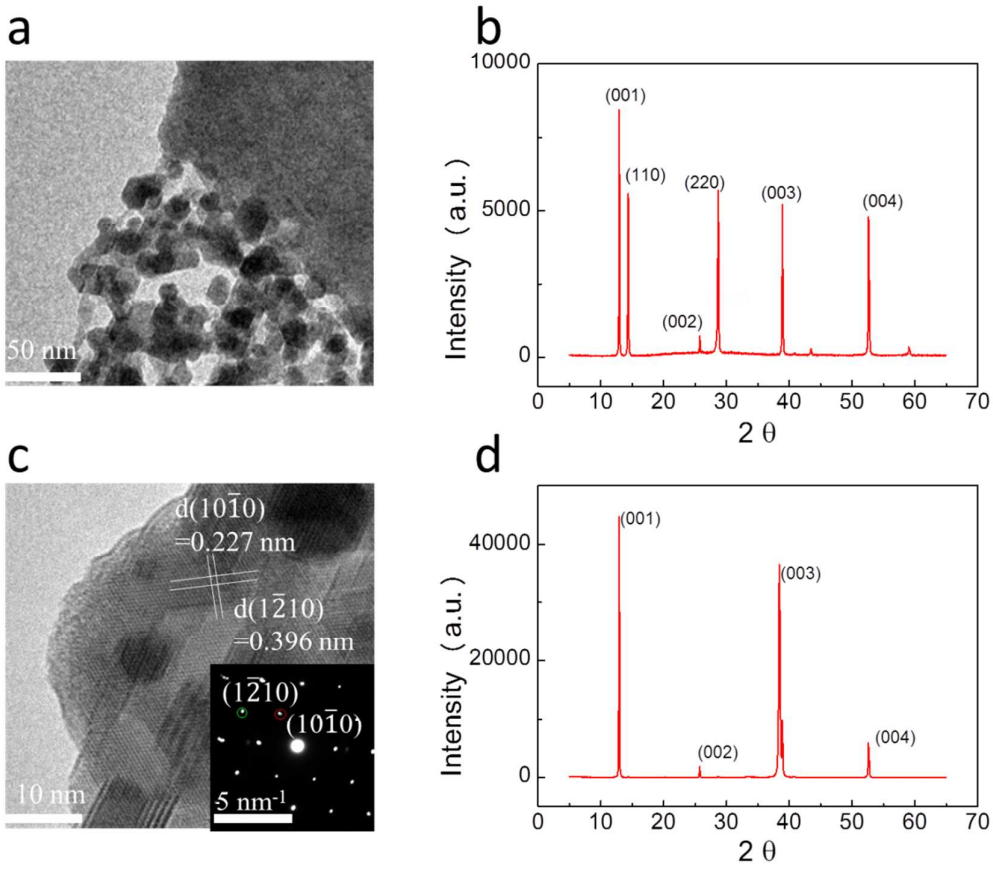

Figure S 3 (a) TEM image of the sample degradation under the electron beam. (b) XRD spectrum of the LPCVD synthesized sample. (c) High-resolution transmission electron microscopy (HRTEM) imagine of the degradation sample. Insert: SAED pattern in figure S3(c). XRD spectrum of PbI_2 nanosheets.

1.4. The optical setup

The optical setup has been shown in figure S4. Photoluminescence of perovskites was excited with a frequency doubled Ti:Sapphire laser (400 nm, using a BBO crystal) from a regenerative amplifier (repetition rate 1 kHz, pulse width 100 fs, seeded by Mai Tai, Spectra Physics).The pumping laser is focused by using a 60×objective lens onto the top surface of the perovskite nanosheets. The emitted light and the corresponding fluorescence microscopy image are collected by the same objective lens coupled with a CCD (Princeton Instruments PIXIS BUV) coupled spectrometer (Acton SpectroPro S2700i) and a camera, respectively. An attenuator and an energy meter were used to tune and measure the pumping density, and a set of filters to filter out 800 nm laser.

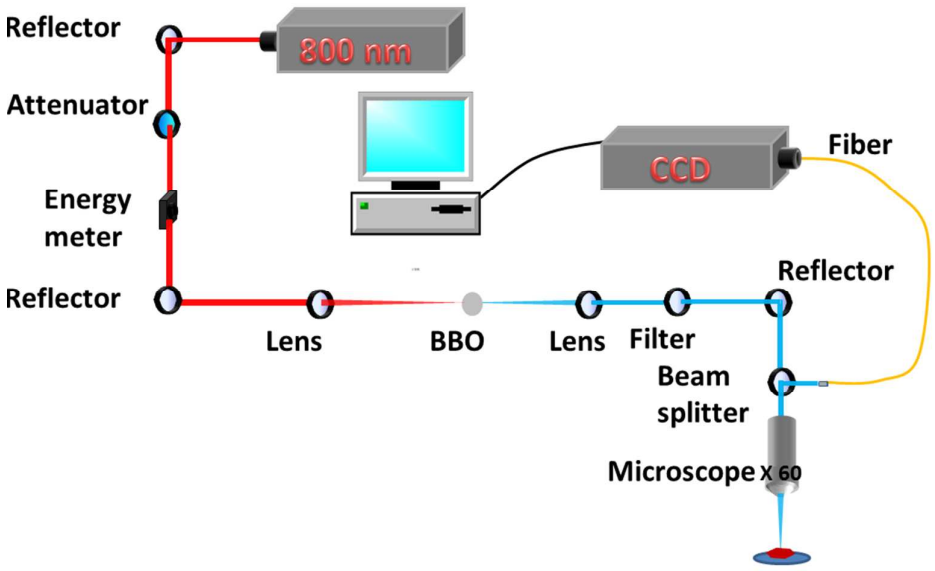

Figure S 4. Schema of optical setup

For the double-pump experiments, as shown in the figure S5, basically, the pulse (same with above) frequency was doubled using a BBO crystal and then split to two beams through a 5:5 beam splitter. One of them passed a delay line and then combined with another through a beam splitter. The optical beam was finally focused on the sample by a 60× objective lens, the emitted light and the corresponding fluorescence microscopy image are collected by the same objective lens coupled with a CCD and a camera, respectively. To make a fair comparison between the photonic and hybrid plasmonic mode lasers, we chose similar normalized pump energy density (1.2 times the respective threshold values). Furthermore, because the responses are nonlinear, we also fixed the power ratio of the two pump pulses at 5:1.

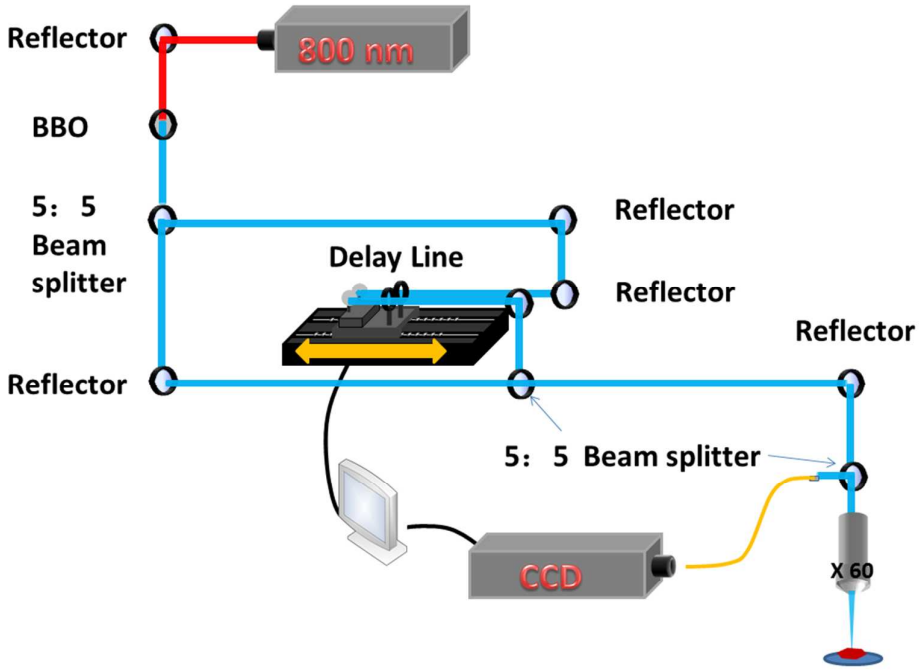

Figure S 5. Schematic picture of optical set-up for double pump experiment.

To confirm the polarization of emission light, we set two polarizers based on above optical setup. Figure S6(a) exhibited the schema of the polarization experiments. Here, the 0° was defined as the direction which the axis of the polarizer norm to the plane (e g, TM mode, with E perpendicular to the plane) to determine the polarization of a single microplates plasmonic laser. While the 0° of the polarizer which determine the emission polarization of the grating spaser array was defined as the direction parallel to the grating strips. Figure S6(b, c) exhibited two set of emission spectrums for vertical and parallel polarization experiments, respectively. Electric field strength of vertical polarization (blue line in figure S6(b)) is much stronger than that in parallel direction (red line in figure S6(b)), characterizing the TM mode. In figure S6(c), the electric field strength norm to the grating strips(red line in figure S6(c)) is much stronger than that in parallel direction(blue line in figure S6(c)), which proved that the dominate electric field is perpendicular to the grating strip, characterizing the plasmonic laser behavior.[4] Notably, the grating schematic in figure S6 (a) was available only when determining the polarization of the grating spaser.

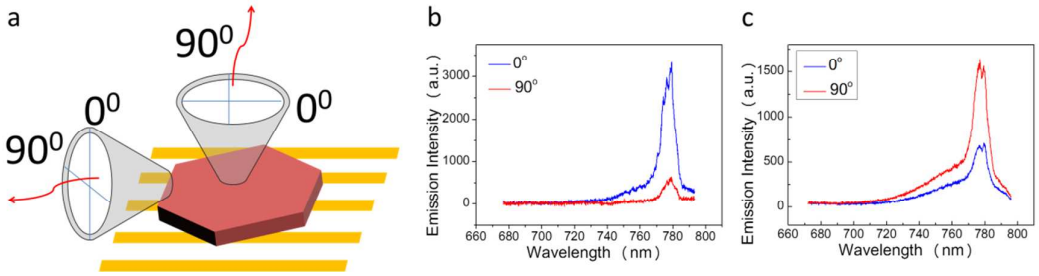

Figure S 6. (a) Schematic picture of optical set-up for polarization experiments. (b) Collected emission spectrum for TM (E field norm to the sample surface) and TE (E field parallel to the sample surface) mode. (c) Collected emission spectrum for E field parallel and norm to the grating strips.

Section-2: Experimental details for wavelength-controllable plasmonic nanolaser and nanolaser array.

2.1 Optical characterization of Photonical mode laser.

Compared with hybrid mode for perovskite/SiO_2/Au configuration. The photonic mode based on perovskite/SiO_2 configuration has several notable features, such as cutoff height, polarization et al. To distinguish the hybrid mode and the photonic mode, we also carefully examined the laser behavior based on perovskite/SiO_2 configuration. As mentioned in the main text, the transverse electric (TE, E is in-plane) has electric field parallel to the metal surface and cannot form the hybrid plasmonic mode, while it can be formed in the photonic mode. First of all, we calculated the effect index a function of perovskite thickness for TE mode. The numerical calculation result (perovskite with 150 nm thickness as an example) for photonic mode has been shown in figure S7 (a), it could be seen that the most of electric field energy stored in the perovskite layer, distinguish to TM mode in hybrid system, which the most of electric field energy stored in the SiO_2 layer. The thickness cutoff for TE mode based on photonic system has been discussed in the main text. Figure S7(b) have shown the AFM imagine of the perovskite microplates with roughness around 4 nm and 220 nm thickness. Then we checked the polarization of the emission laser and the laser intensity as a function of pumping density. The dots in figure S7 (c) shown the dominate electric field direction is parallel to the plane, confirming the TE mode laser in photonic system. Figure S7(d) shown the emission spectrum and figure S7(e)

summarized the output intensity as a function of pumping density. The "S" curve clearly shows the transition from spontaneous emission to amplification and gain saturation and thus the lasing actions in perovskite/SiO_2 nanostructure can be confirmed. The fitting x_0 value for this photonic laser is around 0.028, far smaller than the hybrid plasmonic system. Notably, there are several peaks in the emission output spectrum in figure S7(d). We then summarized the peak gap and the nanosheets side lengths in figure S7(f). It is found that the $\Delta\lambda$ is linearly dependent on 1/L. confirming the WGM mode laser again.

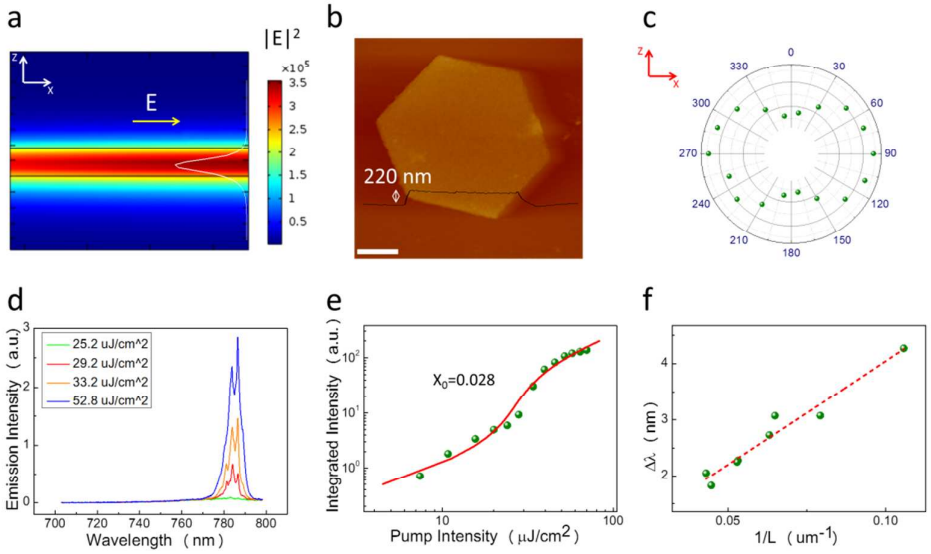

Figure S 7. photonic laser behavior based on perovskite/SiO_2 system. (a) The numerical calculation electric field imagine of perovskite/ SiO_2 system for TE mode(perovskite with 80 nm thickness, n(perovskite)=2.5, n(SiO_2)=1.46). (b) AFM imagine of perovskite setting on mica substrate, scale bar:10 μm. (c) The polarization of the emission laser from side collection. 0^o was set by the direction norm to the perovskite nanosheets. (d) The emission output for different pumping density of the perovskite on mica substrate. (e) Output intensity as a function of pumping density. The fitting x_0 value for the "S" curve is 0.028. (f) $\Delta\lambda$ as a function of 1/L.

2.2. Wavelength-controllable plasmonic nanolaser

As described in the main text, the stoichiometry of synthesized $CH_3NH_3PbI_3$ perovskite microplates can be changed by thermal annealing in a low pressure chemical vapor deposition (LPCVD) with CH_3NH_3Br vapor environment. Different annealing time correspond to different Br/I ratio for $CH_3NH_3PbBr_{3-x}I_x$ perovskite, and different central emission wavelength. To confirm this, we executed the Energy

Dispersive X-ray Spectroscopy(EDX) experiments for perovskite nanosheets on Au/SiO_2 substrate to determine the Br/I ratio (see figure S8(a) as an example). Figure S8(b) described the central emission wavelength as a function of x value for $CH_3NH_3PbBr_{3-x}I_x$. This give us an intuitive result that higher Br/I ratio correspond to shorter emission wavelength.

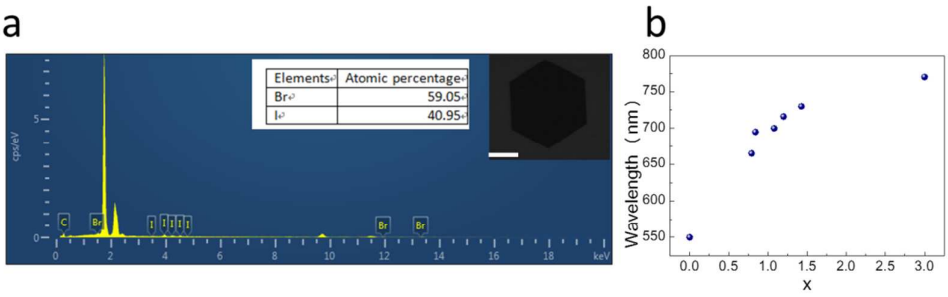

Figure S 8. (a). Energy Dispersive X-ray Spectroscopy for a tested sample. Insert: the corresponding SEM imagine, Scale bar:25 μm. (b). The central emission wavelength as a function of different Br/I ratio for $CH_3NH_3PbBr_{3-x}I_x$ perovskite.

As mentioned in manuscript, the threshold increased as the wavelength blue shift. We confirm this by collect the emission spectrum at different pump intensities. As example, figure S9 shown two blue-shifted emission spectrums for photonic laser and plasmonic laser, respectively. The corresponding integrated output intensity as a function of pumping density shown the transition from spontaneous emission to amplification and gain saturation. And the x_0 value for fitted "S" curve is 0.1 and 0.19, respectively. The higher x_0 confirming the plasmonic laser behavior again since a higher x_0 value giving rise to a high β-factor,[5] even the threshold is increased for blue-shifted plasmonic laser. figure S9(c, f) exhibited polarization emission intensity of photonic and hybrid plasmonic laser, respectively. For photonic laser, the polarization characterizing the TE mode and the polarization of hybrid configuration exhibited the TM mode feature.

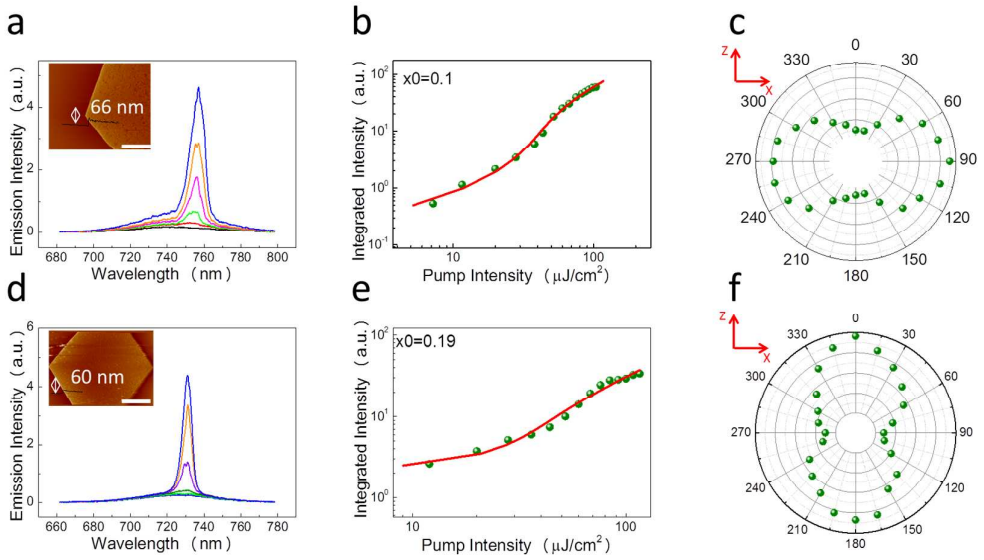

Figure S 9. Blue-shifted emission spectrum (~755 nm for photonic laser (a) and ~730 nm for plasmonic laser(d)) at different pumping density. Insert: corresponding AFM imagine, scale bar 10 μm. (b, d). Corresponding integrated intensity as a function of pumping density, the x_0 value for fitting "s" curve is 0.1 and 0.19, respectively. (c, f) polarization emission intensity of photonic and hybrid plasmonic laser, respectively.

2.3. F-P mode plasmonic nanolaser array

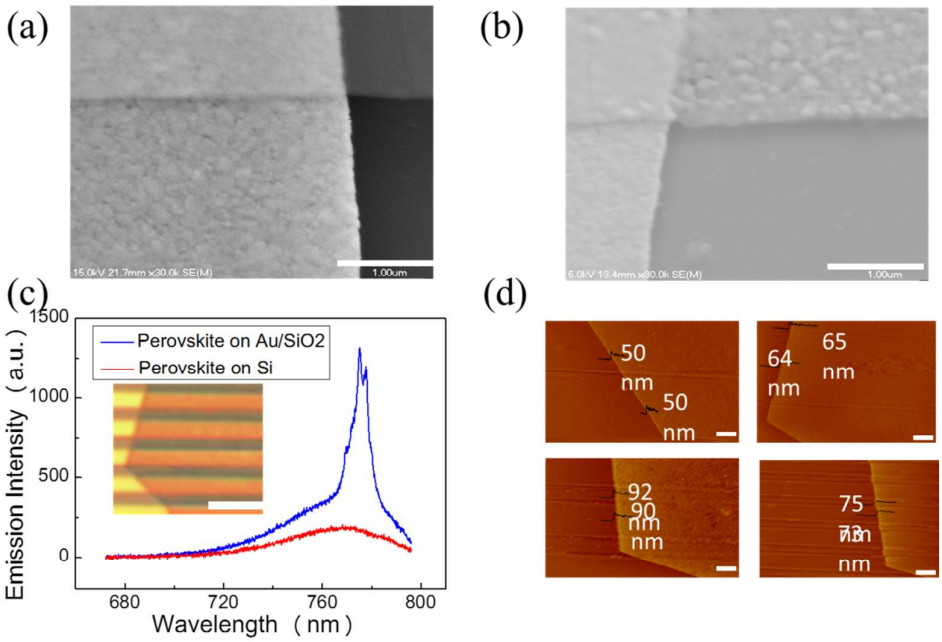

Figure S 10. Tilt-view SEM imagines of (a) PbI_2 nanosheets and (b) perovskite nanosheets covered on the Au/SiO_2 strip. (c) emission spectrums of perovskites on Au/SiO_2 and silicon substrate. (d) AFM imagines for different thickness perovskite nanosheets on Au/SiO_2 stripes.

In the manuscript, we exhibited the FP mode hybrid plasmonic nanolaser array

can be formed in our constructed structures. Here we show the other experimental details, as shown in the SEM and AFM image in the manuscript, the SiO_2-Au strips appear periodically in x-direction, and the Au/SiO_2 stripe protrusion on the surface of a silicon substrate. The perovskite microplates were then transferred on the stripes using a fiber. There is almost no air gap between the perovskite and the strips at the edges, which can be confirmed as shown in figure S10(a) and (b). The tilt-view SEM imagine of PbI_2 nanosheets shows there is small air gap between perovskite and stipe edge, while after the CVD process, as shown in figure S10(b), the air gap disappeared for perovskite nanosheets covered on the Au/SiO_2 strip, which come from the fact that the stress can be released in the heating and cooling process. This can be further confirmed by the AFM imagine as shown in figure 7(a). Figure S10 (d) shows other AFM imagines of thin perovskite nanosheets, the thickness of perovskite nanosheets on stripes and silicon substrate are almost same, which indicates the nanosheets stick the substrate tightly. At the same time, the thickness of these nanosheets are all below the cut-off value for photonic mode. Figure S10 (c) shows the emission spectrums of perovskites on Au/SiO_2 and silicon substrate. It was found that no matter how high the pumping density was, only photoluminescence had been observed due to high loss of silicon (red line in figure S10(c)). While if we pump the Au/SiO_2 part, the emission intensity increased dramatically and the emission spectrum was dominated by the sharp peaks (blue line in figure S10(c)), which prove the conclusion again mentioned above.

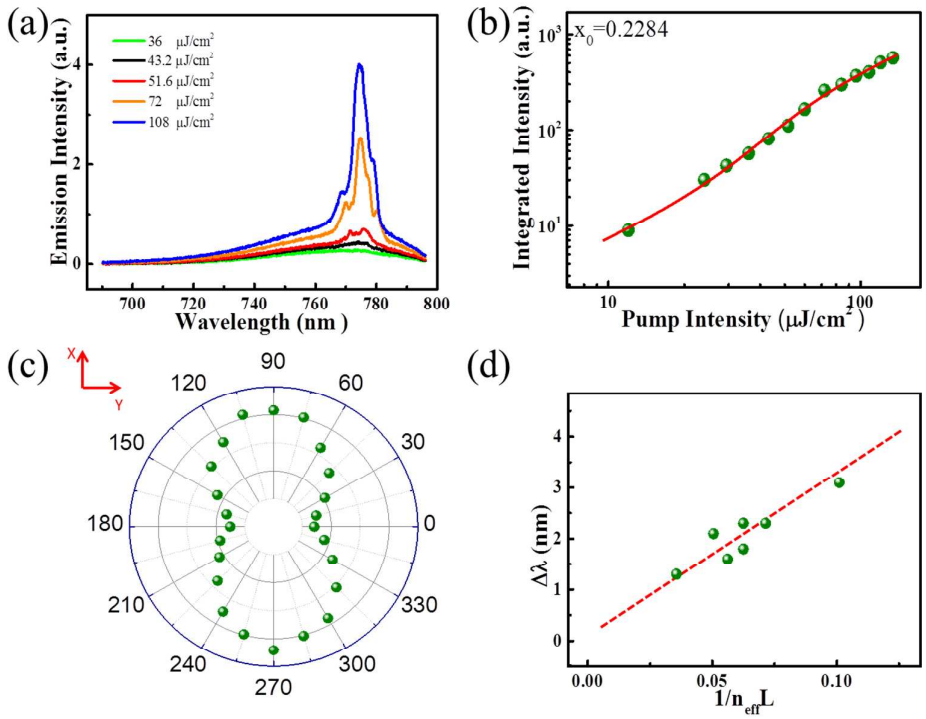

Figure S 11. (a) The emission spectrum and (b) output intensity as a function of pumping density. (c) The polarization of photoemission. (d). Free spectral range as a function of $1/n_{eff}L$

To confirm the FP mode hybrid plasmonic laser generated between two edges of the stripe. We first measured the emission spectrum and verified the polarization. Figure S11(a) and (b) exhibited the emission spectrum and output intensity as a function of pumping density. We then fitted the curve and the corresponding fitting value x_0 is 0.228, which is consistent with previous hybrid plasmonic lasers. Figure S11(c) shows the polarization of the emission, which is perpendicular to the grating strips. Notably, the polarization directions for different configurations are all perpendicular to the grating strips and is independent to the orientation of the nanosheets (see figure S 11). While for a nanowire hybrid plasmonic laser (which shown the FP cavity mode), the polarization direction of a nanowire is along its axis. Since the FP mode can only exist in the direction which perpendicular to the strips, we then conclude the FP cavity formed in the device was the hybrid plasmonic mode.[4] Besides, we found that the free spectral ranges of these samples were all different. This is because that the different grating lattice and thickness of perovskites can give

different optical paths. Figure S11(d) shows the free spectral range as a function of $1/n_{eff}L$. Here n_{eff} is the effective index and L is the width of SiO_2-Au strip. We can see that the mode spacing is linearly dependent on $1/n_{eff}L$. Such kind of relationship matches the equation $\Delta\lambda=\lambda^2/(2n_{eff}L)$ and confirms the generation of Fabry-Perot based plasmonic nanolaser on the SiO_2-Au strip. While we should point out that the "not good liner relationship," on the one hand, may come from the fact that the contact was different for different microplates with different thickness. And on the other hand, this model is generally more accurate for the microplates with same thickness. In our experiments, the samples came from many nanosheets. Due to the thickness of some nanosheet below 50 nm, the dispersion is very intense according to figure 1, which will cause some extra deviation.

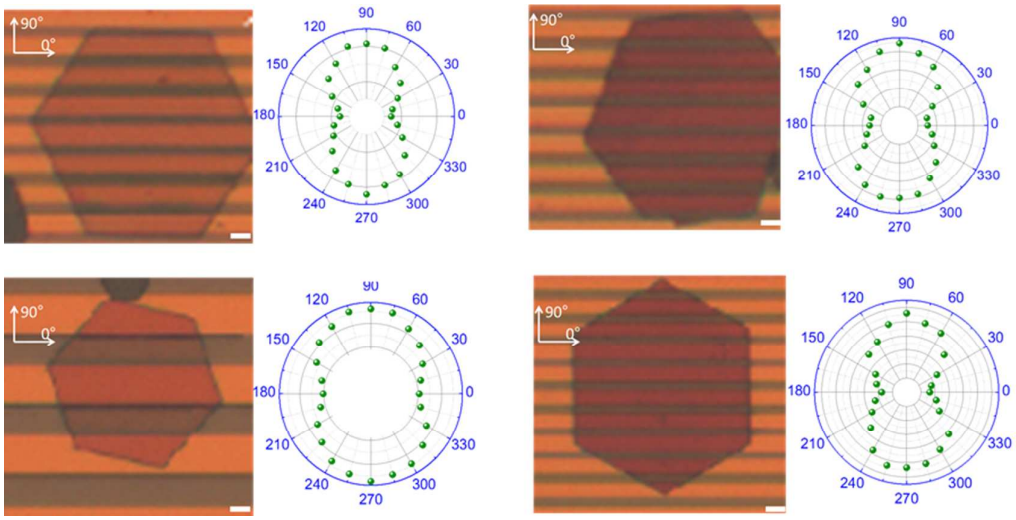

Figure S11. Far-field polarization of grating spasers for different configuration of perovskite on Au/SiO_2 grating. The thickness of the perovskite is 65 nm, 90 nm, 60 nm, 85 nm, respectively. Scale bar: 5 μm. The polarizer locates at the top of samples and 0° was set as the direction which the axis of the polarizer parallel to the grating strips.

In fact, for thicker perovskite microplates, it may suspend on the Au/SiO_2 grating. Figure S12(a) shown the SEM imagine of suspend perovskite microplate on Au/SiO_2 grating and corresponding imagine under irradiation and AFM imagine. It can be seen that the emission area now transferred to the grating edge. Figure S12(b) shown the emission output spectrum and integrated intensity as a function of pumping density

correspond to (a), the x_0 value for fitting curve is 0.02644, which is smaller the grating spaser and close to the photonic mode laser. We contributed this laser was formed by the symmetric configuration composed of air/perovskite/air. As contrast, figure S12(c) shown the SEM imagine of perovskite microplate clinging to Au/SiO_2 grating and corresponding PL and AFM imagines. Now it could be seen that the emission area was exactly the Au/SiO_2 strips. Figure S12(d) shown the emission output spectrum and integrated intensity as a function of pumping density correspond to (c), the x_0 value for fitting curve is 0.136. which is near the grating spaser.

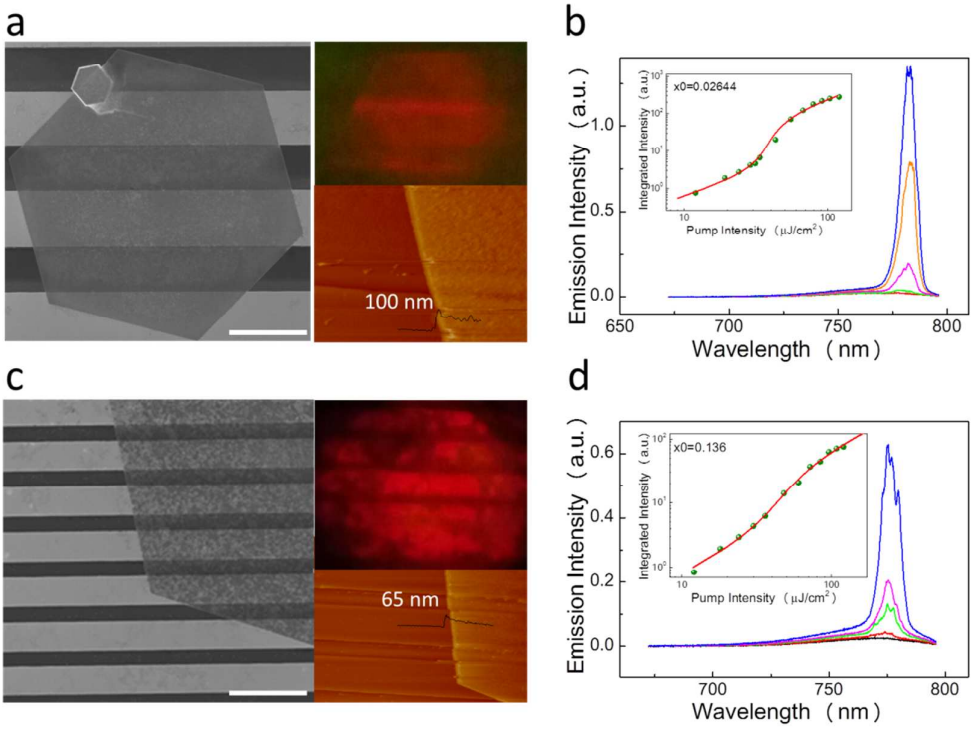

Figure S 12. (a) SEM imagine of suspend perovskite microplate on Au/SiO_2 grating and corresponding imagine under irradiation and AFM imagine. Scale bar: 20 μm. (b) Emission output spectrum and integrated intensity as a function of pumping density correspond to (a), the x_0 value for fitting curve is 0.02644. (c) SEM imagine of clinging perovskite microplate on Au/SiO_2 grating and corresponding PL imagine and AFM imagine. Scale bar: 20 μm. (d) Emission output spectrum and integrated intensity as a function of pumping density correspond to (c), the x_0 value for fitting curve is 0.136.

Lastly, Before LPCVD transfer process, the PbI_2 nanosheets was clinging to the Au/SiO_2 grating. Since the PbI_2 nanosheets could form lasers[6], we then pumped the PbI_2 nanosheets on Au/SiO_2 grating. Figure S13(a) shown the optical imagine of the

sample and the emission spectrum at 120 uJ/cm^2, respectively. Two bright line at the edge of SiO_2-Au strip can be observed in figure S13(a). A emission peak locals at 517 nm can be seen from emission output spectrum in figure S13(b), confirming the onset of Fabry-Perot based plasmonic nanolaser.

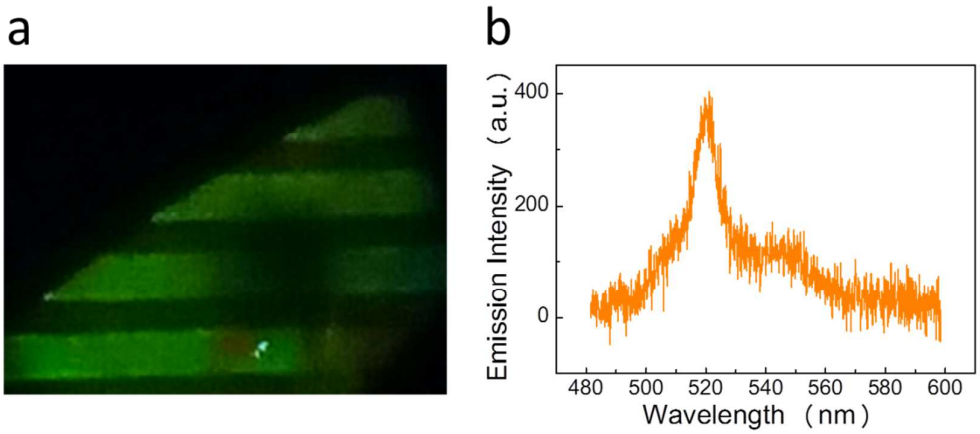

Figure S 13. PbI_2 grating spaser. (a) optical imagine of PbI_2 nanosheet at 120 uJ/cm^2 pumping density. (b) Emission output spectrum corresponding to (a), the emission peak locals at 517 nm.

References:

(1) Brenner, T. M.; Rakita, Y.; Orr, Y.; Klein, E.; Feldman, I.; Elbaum, M.; Cahen, D.; Hodes, G. Conversion of Single Crystalline $PbI_2$to CH3NH3PbI3: Structural Relations and Transformation Dynamics. *Chem. Mater.* **2016**, *28*, 6501-6510.

(2) Cao, D. H.; Stoumpos, C. C.; Malliakas, C. D.; Katz, M. J.; Farha, O. K.; Hupp, J. T.; Kanatzidis, M. G. Remnant PbI_2, an Unforeseen Necessity in High-Efficiency Hybrid Perovskite-Based Solar Cells? *APL Mater.* **2014**, *2*, 091101.

(3) Xing, J.; Liu, X. F.; Zhang, Q.; Ha, S. T.; Yuan, Y. W.; Shen, C.; Sum, T. C.; Xiong, Q. Vapor Phase Synthesis of Organometal Halide Perovskite Nanowires for Tunable Room-Temperature Nanolasers. *Nano Lett.* **2015**, *15*, 4571-4577.

(4) Zhang, Q.; Li, G.; Liu, X.; Qian, F.; Li, Y.; Sum, T. C.; Lieber, C. M.; Xiong, Q. A Room Temperature Low-Threshold Ultraviolet Plasmonic Nanolaser. *Nat. Commun* **2014**, *5,* 4953.

(5) Oulton, R. F.; Sorger, V. J.; Zentgraf, T.; Ma, R. M.; Gladden, C.; Dai, L.; Bartal, G.; Zhang, X. Plasmon Lasers at Deep Subwavelength Scale. *Nature* **2009**, *461*, 629-632.

(6) Liu, X.; Ha, S. T.; Zhang, Q.; de la Mata, M.; Magen, C.; Arbiol, J.; Sum, T. C.; Xiong, Q. Whispering Gallery Mode Lasing From Hexagonal Shaped Layered Lead Iodide Crystals. *ACS Nano* **2015**, *9*, 687-695.